An investigation into supersonic shallow swept cavity flows

B. Reim, C. Panetta, E. Samanes, S. Gai, J. Milthorpe and H. Kleine
School of Aerospace, Civil and Mechanical Engineering,
University of New South Wales
Australian Defence Force Academy,
Canberra, Australia

ABSTRACT

An experimental investigation was conducted to determine the flow characteristics of shallow swept cavities at a free-stream Mach number of 2. The investigation described herein focused on obtaining information on both time-averaged and time-dependent flow features. The data consisted of steady and unsteady pressure measurements as well as some surface oil and schlieren flow visualisation. The effective length-to-depth ratios l/d of cavities investigated ranged between 5·65 and 8 for shallow 'open' cavities and between 11·31 and 16 for 'closed' cavities. The cavity sweep angles were 0°, 15° and 45°. The results of the swept cavities, when compared to the datum cases of the straight (0°) cavities, showed some distinct differences. With regard to time-averaged flow characteristics, in an open swept cavity ($5{\cdot}65 < l/d < 8$), the flow displayed quasi-open flow behaviour, distorted by the spanwise cross flow within the cavity. In the case of the closed swept cavity ($11{\cdot}31 < l/d < 16$), flow features resembling the 'closed' to 'transitional closed' cavity flow types were seen to exist simultaneously across the span. Unsteady pressure data indicated that for an open cavity at 15° sweep angle, the discrete frequencies observed were similar to those of a straight open cavity. In contrast to this, at 45° sweep angle, the frequencies were broadband with no discrete frequency across the cavity length. For the closed cavity, the frequencies were all broadband irrespective of the sweep angle. The investigation also showed that the influence of the sweep angle on the pressure drag of the cavity strongly depends on the type of cavity flow: a sweep angle increase from 0° to 45° approximately doubled the pressure drag for an open cavity, while it led to a drag reduction of about 37% for the closed cavity.

NOMENCLATURE

$\overline{C}_D$	time-averaged drag coefficient
C_p	pressure coefficient
d	depth of cavity
f	oscillation frequency
l	streamwise length of cavity
l_{eff}	effective length of cavity (shortest distance between leading and trailing edge)
M	Mach number
M_n	flow Mach number normal to the leading cavity edge
M_∞	free stream Mach number
n	mode number (n = 1, 2, 3 …)
p	pressure
$\overline{p}_f$	average pressure on front cavity face
$\overline{p}_r$	average pressure on rear cavity face
p_∞	free stream pressure
p_{rms}	root mean square value of pressure amplitude
p_r	reference sound pressure
SPL	sound pressure level
U_c	convection velocity
U_∞	free stream velocity
x	co-ordinate in streamwise direction
y	co-ordinate in the spanwise direction
w	width of cavity
z	co-ordinate perpendicular to cavity floor
β	phase lag
δ	boundary layer thickness
γ	ratio of specific heats (γ = 1·4 for air)
ψ	sweep or yaw angle of the cavity

Paper No. 3284. Manuscript received 29 February 2008, revised 8 May 2008 accepted 28 July 2008.

https://doi.org/10.1017/S0001924000002542 Published online by Cambridge University Press

1.0 INTRODUCTION

Designers of missiles, re-entry vehicles, and aircraft encounter a variety of design problems related to the flow characteristics in and around cavities. A number of investigations of such problems have been conducted over the years to increase our understanding of cavity flow fields at subsonic through to hypersonic speeds. The results obtained at supersonic speeds are of particular interest for the design of internal or semi-submerged weapons bays of military aircraft. The successful delivery of armaments from internal weapons bays requires a sound knowledge of the cavity flow field to prevent weapon and store release problems [1].

It has also been well known that the presence of cavities on aircraft and missile structures gives rise to drag and, more importantly, to structural fatigue and buffeting due to pressure oscillations and far field noise radiation, both of which exert a baleful influence on airframe structure and environment. The importance of alleviating noise and vibrations has recently taken on an added significance with the projected development of the so-called 'Silent Aircraft' for the 21st century [2]. Besides, the cavity fluid dynamic behaviour by itself has for a long time attracted the attention of aerodynamicists and acousticians because of its intrinsic fundamental interest [3,4,5].

A cavity is called shallow if its depth d is much smaller than its length l ($l/d \geq 5$)[6] (see Fig. 1(a) for an illustration of the nomenclature and variables used here). Two fundamental types of cavity flow fields exist depending on the length-to-depth ratio l/d of the cavity[7,8,9]. If this ratio is less than about 10, the cavity is said to be of the 'open' type, and if it is greater than about 13, the cavity is considered to be of the 'closed' type. Cavities with $10 < l/d < 13$ are called 'transitional' and are further subdivided into 'transitional open' and 'transitional closed'.

The rectangular open cavity is characterised by a free shear layer, which is formed as a result of the flow separating from the cavity leading edge and reattaching to the cavity trailing edge, essentially bridging the cavity. The mean pressure distribution in the cavity is relatively constant over most of its length, but shows a rise at the cavity trailing edge due to the shear layer reattachment. The unsteady flow in the open cavity exhibits distinct acoustic tones through the production of self-sustaining pressure oscillations within the cavity[6,8,10].

In a closed cavity, the separating shear layer from the cavity leading edge attaches to the cavity floor after passing through an expansion fan at the leading edge corner and a recompression shock at attachment. The attached shear layer then separates near the trailing edge and causes a separation shock before reattaching at the trailing edge prior to undergoing an expansion. The resulting mean pressure distribution starts with a negative value at the leading edge, increases up to the point of shear layer attachment, then exhibits a plateau, which covers a substantial region of the cavity floor, and finally shows a large increase due to the shear layer impingement on the trailing edge. The unsteady pressures in the closed cavity exhibit a broadband spectrum unlike the resonant behaviour of the open cavity.

For the transitional type cavity, the steady pressure distribution is characterised by a nearly constant pressure region that can cover up to 50% of the cavity length, followed by a monotonically increasing pressure up to reattachment of the shear layer at the cavity trailing edge. The pressure distributions for a transitional open and a transitional closed cavity are largely similar, the main difference being the steeper increase of pressure in the transitional closed case, which is caused by the attachment of the shear layer on the cavity floor. Furthermore, the pressure values may stay positive throughout the cavity in a transitional open cavity, while the values close to the leading edge are negative in a transitional closed cavity. Tracy and Plentovich[8] have shown that transitional closed cavities do not typically exhibit resonant unsteady flow behaviour. This is because the impingement of the separated shear layer on the cavity floor inhibits the generation of acoustic tones.

Typical steady pressure profiles for the various types of cavities are given in Section 3.5 together with the distributions measured in this investigation.

While the basic flow characteristics pertaining to straight cavities (wherein both the cavity leading and trailing edges are normal to the direction of the oncoming flow) are now fairly well understood, similar information is sparse in regard to swept cavities, where the leading and trailing edges of the cavity are at yaw to the direction of the oncoming flow, especially at supersonic speeds. Studies by Tracy and Plentovich[8] have considered the effects of yaw but their investigations were restricted to a yaw angle of only 15° and a single free-stream Mach number of $M_\infty = 0{\cdot}9$. The work by Disimile and Orkwis[11], done at Mach number $M_\infty = 2$, describes the flow in a deep open cavity ($l/d = 2$) and concentrates on the variation of sound pressure levels within the cavity with changes in yaw angle. The work of Toy *et al*[12] describes shear stress levels using a liquid crystal technique and tries to correlate the shear stress data with sound pressure levels of Ref. 11. However, both these studies do not give detailed pressure data, neither steady nor unsteady. The present paper attempts to fill this gap and also provides information on features such as cavity pressure drag for a swept cavity, both short (open) and long (closed).

2.0 EXPERIMENTAL TECHNIQUES

The experiments were conducted in a blow-down supersonic wind tunnel of cross-section 156mm (height) and 90mm (width) at a free-stream Mach number of $M_\infty = 2$. A sharp-edged flat plate 280mm long and 8mm thick and spanning the full width of the tunnel was mounted along the axis of the tunnel as a splitter plate, which contained the cavity model (see Figs. 1(b), (c)). For steady pressure measurements, a cavity model equipped with an array of pressure tappings was installed. The three cavity yaw angles, 0°, 15°, and 45°, were achieved by using interchangeable inserts to define the cavity geometry. For each of the investigated length-to-depth ratios l/d of the cavities, the distance between the leading edge of the flat plate and the leading edge of the cavity along the centreline of the model was constant. The cavity depth was 4mm. Two length-to-depth ratios l/d of the cavity were used in the tests. The short swept cavity, with a streamwise length-to-depth ratio l/d of 8 was equivalent to an open straight cavity. The long swept cavity had a streamwise length-to-depth ratio l/d of 16 and was equivalent to a closed straight cavity. Because of the sweep, the 'effective' length-to-depth ratios† of the cavities for sweep angles 15° and 45° were 7·7 and 5·65 in the case of the open cavity and 15·45 and 11·31 in the case of the closed cavity, respectively. According to Tracy and Plentovich[8], the length-to-depth ratio of 11·31 borders on the 'transitional closed' regime.

Pressure tappings were located along four separate longitudinal rows equally spaced either side of the cavity centreline (rows #2 and #3 in the mid-span region and rows #1 and #4 towards the sidewalls) so that both spanwise and streamwise pressure data on the cavity floor could be obtained. In all, 26 pressure tappings were available on the cavity floor. In addition, eight pressure tappings across the span were provided on both the front and rear face of the cavity to yield the spanwise pressure distribution on these surfaces. This enabled us to experimentally determine the pressure drag. The pressures were measured by a Druck 3·5 bar pressure transducer via a Scanivalve with the free-stream static pressure as a reference. The Scanivalve was operated by MATLAB software via a solenoid controller. The pressure values are represented as coefficients of pressure C_p and the error in C_p due to inherent measurement inaccuracies is ±0·0025.

The unsteady pressure measurements were carried out in different cavity models that had the same dimensions and geometry as the ones used for the steady measurements, but were equipped with five fast response miniature Kulite gauges (XCQ-062). One transducer was located on each face of the cavity and three on the cavity floor, in streamwise direction along the centreline of the model. The output

† The effective length of the cavity, l_{eff} is defined as the shortest distance between leading and trailing edge of the cavity. For a streamwise cavity length l and a sweep angle ψ, $l_{eff} = l \cos\psi$ (see Fig. 1(a)).

https://doi.org/10.1017/S0001924000002542 Published online by Cambridge University Press

from the transducers was fed to a differential amplifier at a sampling rate of 200kHz and record length of four seconds. The signals were processed using a MATLAB software that included a low-pass fourth order Butterworth filter with a cut-off frequency of 3kHz. The frequency resolution was 50Hz. The pressures are presented in the form of Sound Pressure Level (SPL) using the conventional reference pressure (20μPa) that corresponds to the threshold of hearing as is customary in acoustics:

$$SPL = 20\log_{10}\left(\frac{p_{rms}}{20\mu\,\mathrm{Pa}}\right) \quad \ldots (1)$$

Here SPL is given in dB, p_{rms} is the root mean square value of the pressure amplitude measured in Pa, and 20 μPa is the reference sound pressure defined above.

The results are expressed as power spectra for the signal measured by each transducer. The resolution of the data resulted in an error in SPL of ± 0·1dB.

Direction-indicating colour schlieren images – typically six to eight frames per tunnel run – were obtained of the flow in the cavities using a flash light source with a pulse width of 200μs. For the visualisation of the flow in swept cavities, the test beam of the schlieren system traversed the test section parallel to the faces of the cavity so that an unobstructed view of the full length of the cavity could be obtained, similar to the datum case of the straight cavity. The size of the test section windows, however, only allowed us to visualise cavities with a maximum yaw angle of 15°.

Surface oil flow visualisation experiments were conducted using a mixture of light vegetable oil, kerosene, and titanium dioxide (4:1:3 by volume) and a few drops of oleic acid added to the mixture to prevent coagulation. The mixture was applied to the cavity surface using an artist's brush so that a smooth thin layer of the mixture could be achieved.

3.0 RESULTS AND DISCUSSION

3.1 The boundary layer at the cavity leading edge

The separating boundary layer at the cavity leading edge is known to influence the characteristics of the cavity flow. Charwat *et al*[7] point out that the ratio of the separating boundary layer thickness to cavity depth, δ/d, is an important parameter and that the effect of increasing the boundary layer thickness for a constant depth cavity is to smooth out the adverse pressure gradient effects in the cavity and increase the skin friction on the cavity floor. Secondly, Zhang and Edwards[10] suggest that the boundary layer, through the amplification of vortical disturbances by the separated shear layer, plays an important role in sustaining the oscillatory mechanism within the open cavity, although oscillatory frequency prediction models do not take into account the finite thickness of the boundary layer.

In the present experiments, the effect of boundary layer thickness was studied by using a sandpaper roughness strip attached to the flat plate 12mm from its leading edge. The oncoming boundary layer at the cavity was measured by means of a pitot tube with 0·45mm opening, located 13mm ahead of the cavity leading edge. It was found to be turbulent and about 2·2mm thick without roughness and 3·5mm with roughness. The correction for displacement effect was less than a tenth of the total boundary-layer thickness and hence was considered insignificant. As will be described later, in the present experiments the boundary layer thickness had only a minor effect both on the steady pressure distributions and cavity pressure drag. The unit Reynolds number at the cavity was 37×10^6 per metre. Using the momentum thickness as reference length scale, the Reynolds number varied between $6{\cdot}29 \times 10^3$ and $10{\cdot}01 \times 10^3$. The measured boundary layer thickness values agreed well with those calculated for a turbulent boundary layer using the criterion of Crocco and Lees[13].

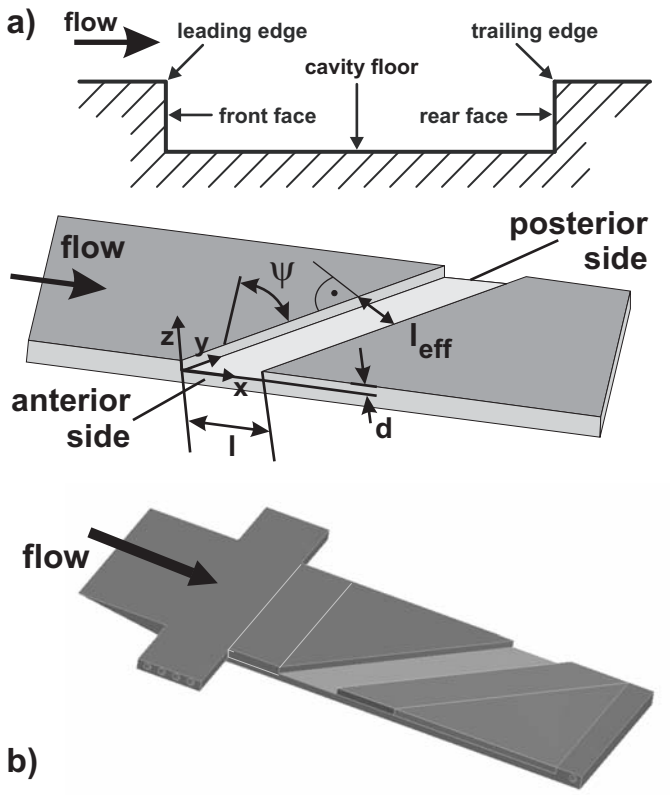


Figure 1.
(a) Cavity geometry and nomenclature.
(b) Swept cavity model arrangement, showing removable inserts to change sweep angle and length-to-depth ratio.
(c) Integration of swept cavity model in test section.
The front side wall of the test section has been removed for clarity.

3.2 Unsteady pressures

All the unsteady pressure data described below pertain to those obtained without increased surface roughness.

For straight cavities, the fundamental frequencies of oscillations in longitudinal, spanwise and transverse direction are characterised by cavity length (l), width (w), and depth (d)[6]. It is known[10,14] that for shallow cavities ($l/d \geq 5$), the longitudinal mechanism dominates the oscillations in the cavity. For the present experimental conditions, the fundamental longitudinal frequency is calculated to be 5·4kHz.

https://doi.org/10.1017/S0001924000002542 Published online by Cambridge University Press

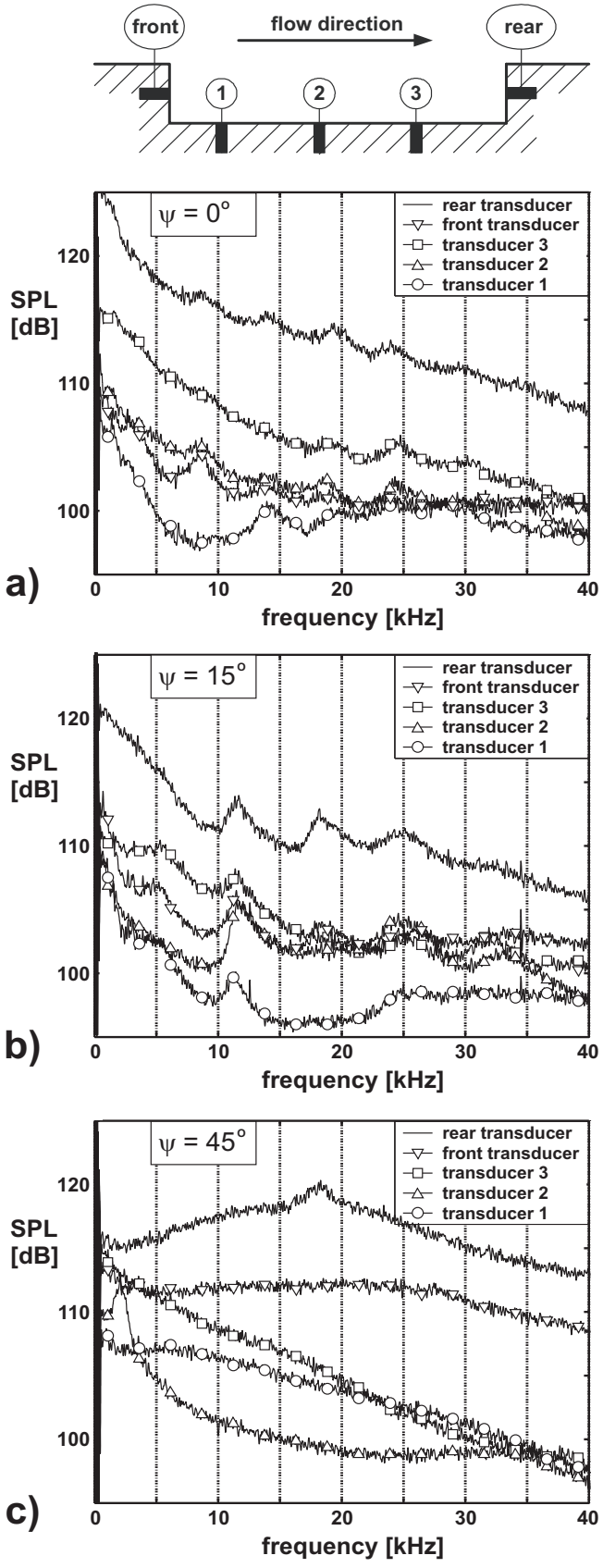


Figure 2. Sound pressure level spectrum in open cavities (l/d = 8) for nominal free-stream flow Mach number M_∞ = 2
a) straight cavity, b) swept cavity, ψ= 15°, c) swept cavity,ψ= 45°

The corresponding values for lateral and transverse oscillations are 1·9kHz and 42·3kHz, respectively. The non-dimensional frequency based on the stagnation speed of sound in the cavity is 0·5.

3.2.1 Open cavity results

ψ = 0°

The power spectrum signals of each transducer for the open cavity flow with zero sweep (Fig. 2(a)) reveal the existence of discrete resonant frequencies at 8kHz, 14kHz, 19kHz, 23kHz, and 30kHz, but the peaks are fairly weak. While most of the modes are present at the rear face, they are less predominant or distinct on the front face and the floor of the cavity. These signals can be contrasted with the results of Tracy and Plentovich[8] where they are sharper and their amplitudes are higher. This may be attributed to the differences in Mach number and the separating boundary layer thickness in the two experiments. Although the length-to-depth ratios in the two cases are similar, in the experiments of Tracy and Plentovich[8] the Mach number was transonic (M_∞ = 0·9) and the ratio of boundary layer thickness to cavity depth (δ/d) was 0·2. In the present investigation, the Mach number is supersonic (M_∞ = 2) and the ratio δ/d is 0·55. Thicker shear layers tend to smooth out the gradients in the flow[10]. As is to be expected, the amplitude is much higher on the rear face because of the impingement of the shear layer.

ψ = 15°

With the 15° swept cavity (Fig. 2(b)), the spectra are generally similar to the zero sweep case, but they appear much sharper. However, the frequency peaks do not exactly align with those of the straight cavity. Particularly, the rear and front face transducers exhibit peaks at 11·5kHz, 17kHz and 25kHz while the floor transducers show distinct peaks only at 11·5kHz. This change in frequency is due to the effect of sweep as the frequency of a mode is a function of the flow path length across the cavity. One might expect the flow path length to vary as (l/Cosψ). In addition to the sweep angle effect, there are the sidewall effects which reduce the flow path length in their vicinity, thus smearing the mode peaks and also reducing the pressure amplitude. Comparison with Fig. 2(a) shows that two of the modes (8kHz and 23kHz) visible at zero sweep are not resolvable at 15° sweep. This situation is accentuated at higher sweep angles as shown below.

ψ = 45°

With 45°sweep (Fig. 2(c)), the spectra are all broadband. The rear face trans ducer spectrum shows a peak at 18kHz but not a sharp discrete tone. The front face transducer shows approximately constant pressure amplitude across the frequency range. The floor transducers all show continuously decreasing pressure amplitude with increasing frequency. The reason for the frequency peak at 2kHz seen with transducer #2 is not clear. The rather random nature of the spectra with 45° sweep would indicate a complex flow resulting from strong cross flows and sidewall interaction.

3.2.2 Closed cavity results

ψ = 0°

Figure 3(a) shows the results for a straight closed cavity. The spectra are all broadband indicating no discrete frequencies. This is consistent with the fact that in a closed cavity oscillatory behaviour is inhibited, because the flow first attaches and subsequently separates from the floor. It is also noted that the pressure amplitudes on the rear of the cavity are significantly higher than those at the front. Similar to the open cavity case, this is caused by the impinging shear layer.

ψ = 15°

Figure 3(b) shows the data for the 15° sweep angle. Transducers #1 and #2 near the leading edge and the transducer on the front face

https://doi.org/10.1017/S0001924000002542 Published online by Cambridge University Press

show discrete frequencies at 2kHz and 5kHz. By contrast, further downstream the spectra are broadband although the transducer on the rear face shows a weak peak at 5kHz. Similar to the straight cavity case, the amplitudes at the rear are much higher than those at the front. It is possible that the low discrete frequencies at the front may be the result of the corner vortex in the separated region at the front face, which is observed in a closed cavity flow. This vortex may become unstable as a result of cross flows resulting from the sweep. This is only a conjecture at the present time.

ψ = 45°

With the 45° swept cavity (Fig. 3(c)), again, the spectra are broadband in the rear part of the cavity. Again, the transducer #1 at the front shows a slight peak at 2kHz as in the 15° case. We also note that its spectrum is markedly different from the other two front transducers. As discussed above with reference to the 15° swept cavity, the corner vortex is now subject to much stronger cross flows resulting in higher unsteadiness in the separated region at the front.

3.3 Analysis of oscillatory modes

The above frequencies and modes can be compared with theoretical predictions based on a modified Rossiter's formula[14], *viz*.

$$\frac{f\,l}{U_\infty} = \frac{n-\beta}{\frac{U_\infty}{U_c} + \frac{M_\infty \mathrm{Cos}\psi}{\sqrt{1+\left(\frac{\gamma-1}{2}\right)M_\infty^2}}} \qquad \ldots (2)$$

where;

n = 1, 2, ... is the mode number, β is the phase lag which is dependent on cavity depth, f is the oscillation frequency, U_c is the convection velocity, and l is the cavity length. U_∞ and M_∞ are the free-stream velocity and Mach number, respectively, and γ is the specific heat ratio. ψ is the sweep angle. The factor β/f represents the total time delay between (*i*) the arrival of a vortex at the trailing edge and the emission of the acoustic pulse and (*ii*) the arrival of this pulse at the leading edge and the subsequent release of new vorticity. For high Mach numbers and shallow rectangular cavities, experimental evidence[14] suggests that β ≈ 0·25 and $U_c/U_\infty \approx 0{\cdot}6$ independently of the temperature of the free-stream, the cavity width and the Reynolds number based on the cavity length.

Figure 4 shows the comparison between the theoretical Strouhal numbers (as calculated above) and the experimental ones obtained from the spectra. It is seen that the spectra only show frequencies that largely correspond to the second, third, and fourth Rossiter modes (n = 2, 3, 4). The agreement between the experimental and theoretical values is very good for the modes n = 2, 3, 4 in the case of the straight shallow cavity, but with the introduction of sweep the discrepancies become large. The data suggest a trend towards a small increase in Strouhal number with sweep for a given mode as Eq. (2) predicts, but the results are too few to draw any definite conclusion. It should be noted, however, that the frequency is inversely proportional to the cavity length and decreases with Mach number[6]. Noting that, with sweep, the effective cavity length and also the effective Mach number decrease (the 'effective' values are the streamwise values multiplied by cosψ), a small increase in the magnitude of the Strouhal number is possible. It was found that the agreement between theoretical and experimental values was marginally better if the value β = 0·1 was used rather than β = 0·25. The value of β = 0·1 has been suggested by Zhuang *et al*[15].

3.4 Sound pressure levels

Figure 5 shows the sound pressure levels averaged over the frequency domain as a function of the transducer location on the cavity floor and the cavity faces for both open and closed cavities. For the open cavity, there is a small rise (~4dB) in the average SPL along the floor, regardless of the sweep. On the front and rear

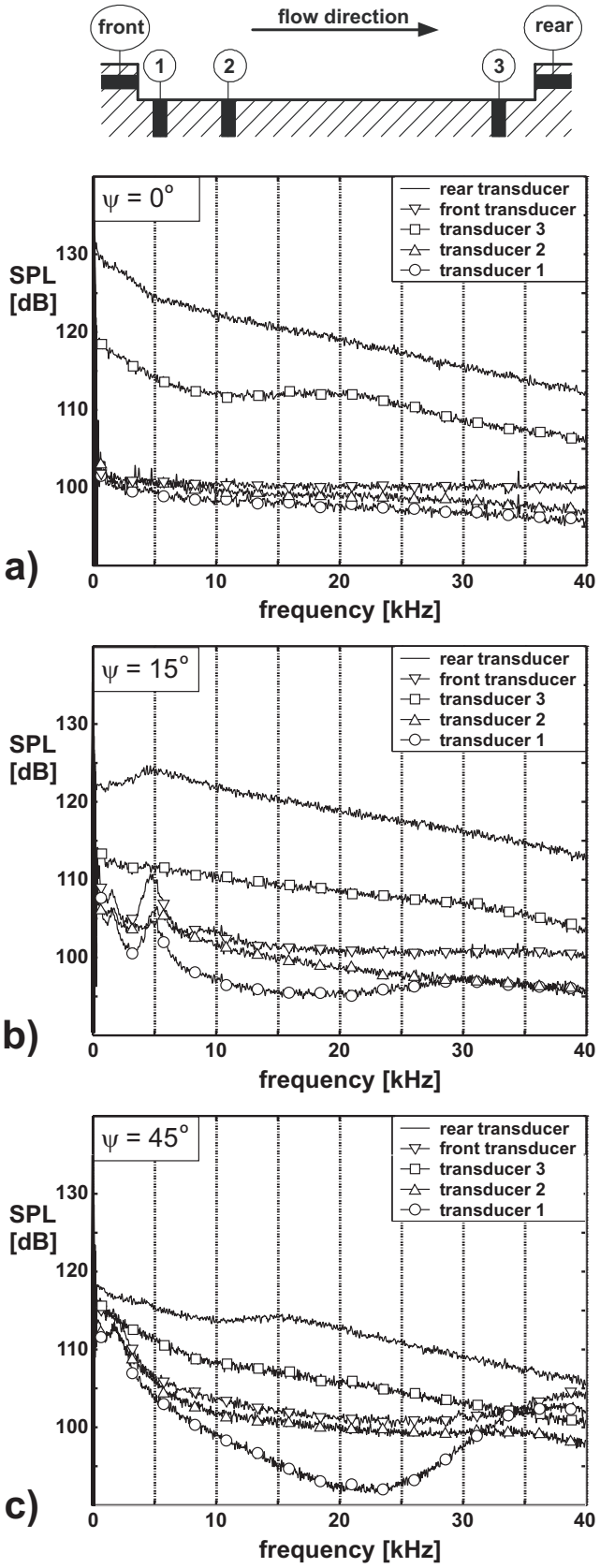


Figure 3.
Sound pressure level spectrum in closed cavities (l/d = 16) for nominal free-stream flow Mach number M_∞ = 2
a) straight cavity, b) swept cavity, ψ = 15°, c) swept cavity, ψ = 45°.

https://doi.org/10.1017/S0001924000002542 Published online by Cambridge University Press

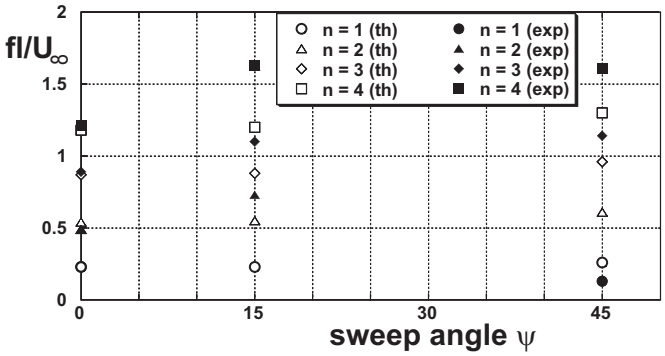


Figure 4. Comparison between experimental and theoretical frequencies (expressed as Strouhal numbers) as a function of sweep angle.

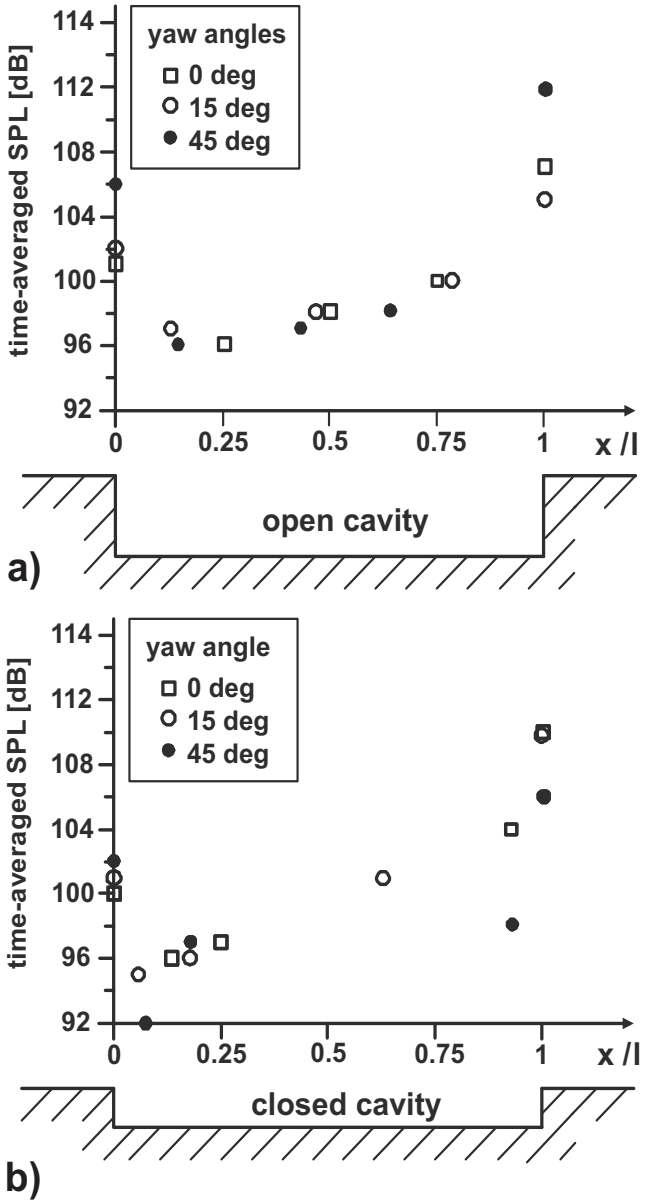


Figure 5. Comparison of sound pressure levels in straight and swept cavities.

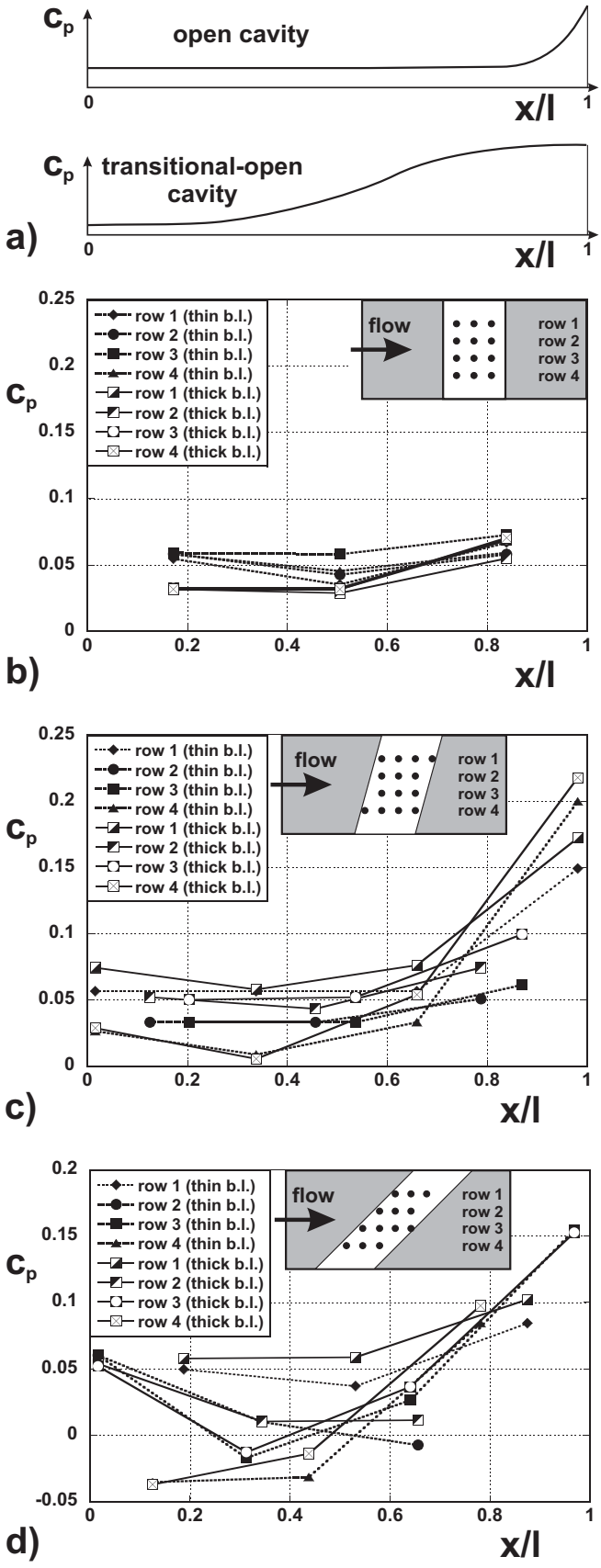


Figure 6. Steady pressure distribution in open cavities (l/d = 8, M_∞ = 2) for thick and thin boundary layers (a) schematic of expected distributions for open and transitional open cavities[8], (b) straight cavity, (c) swept cavity, ψ = 15°, (d) swept cavity, ψ = 45°.

https://doi.org/10.1017/S0001924000002542 Published online by Cambridge University Press

faces, however, the average SPL is affected by the sweep (an increase of about 3 dB is seen on each side when the sweep angle is increased from 0° to 45°). With the closed cavity, on the other hand, the results for the straight and 15° swept cavities show a similar and consistent increase in SPL along the cavity floor, but those with 45° sweep deviate from this trend. Particularly, the average SPL values at the rear face are lower. This is because at this sweep angle, the flow is likely to be dominated by strong cross flows in the spanwise direction which weaken the effect of shear layer impingement at the trailing edge. The strong presence of cross flows was verified in experiments using oil flow visualisation as will be shown later.

3.5 Steady pressures

Figures 6(b), 6(c), and 6(d) show streamwise pressure distributions on the cavity floor along four longitudinal rows of pressure tappings. These rows were equally spaced on either side of the cavity centreline. Rows #2 and #3 were in the mid-span region and rows #1 and #4 towards the sidewalls. Row #1 was on the posterior side and row #4 on the anterior side. The pressure distributions are expressed in terms of pressure coefficient C_p and the streamwise distance x from the leading edge of the cavity is normalised by the cavity length l (Fig. 6(a)). Results for both thick and thin boundary layers are shown for comparison. Depending on the cavity configuration and sweep angle, each row could accommodate three to six pressure tappings spaced equally across the span. The pressure distribution grid on the cavity floor for the open cavity case is, therefore, somewhat coarse. The results are, however, indicative enough to draw reasonable conclusions. In these figures, the discrete data points obtained from the measurements are connected by straight lines to highlight general trends rather than to illustrate a continuous pressure distribution along the cavity.

3.5.1 Open cavity results

ψ = 0°

Figure 6(b) shows the results for the straight cavity. Considering the thin boundary layer (without the surface roughness) results first, we note that the pressures on rows 1, 2, and 4 show an initial decrease before increasing at the trailing edge due the shear layer impingement, while the pressures on row 3 (in the mid-span region) show the typical open cavity pressure distribution[8]. While rows 1 and 4 are towards the side walls and so could possibly be affected by side wall boundary layer effects, the reason for the pressures on row 2, which is in the mid-span region, being different from those in row 3 is not immediately obvious. It should also be pointed out that the cavity aspect ratio w/d (w is the spanwise width of the cavity) is 22·5 in these tests compared to 16 in the experiments of Tracy and Plentovich[8] and 7·6 in the investigations of Zhang and Edwards[10].

Considering the spanwise variations, we note that near the front face, the pressures are all nearly the same indicating good two-dimensionality. At the rear, there are some differences but they are not large. Midway through the cavity, however, there are more pronounced differences indicating some three-dimensional flow effects.

With the thicker boundary layer, the results are all consistent with the typical open cavity pressure distribution and the flow seems reasonably two-dimensional. The other notable difference compared to the thin boundary layer data is that the pressures from the front face to halfway along the cavity length are much lower. This is the effect of the thicker boundary layer which smoothes out the pressure gradient effects[7,10].

ψ = 15°

Figure 6(c) shows the results with 15° sweep angle and these data are consistent with the observation that for small sweep angles the behaviour is not too dissimilar to the straight open cavity[8], at least in the mid-span region. For both boundary-layer thicknesses, the pressure distributions are typical of straight open cavity behaviour. The mid-span pressures (rows 2 and 3) for both boundary layer cases are nearly constant up to halfway through the cavity length before increasing as a result of shear layer impingement at the rear face. The pressures on rows 1 and 4, however, which are towards the side walls, show large increases at the rear face (it ought to be kept in mind, though, that due to the rectangular array arrangement of the pressure tappings, the corresponding pressure ports in rows 1 and 4 are closer to the rear cavity face than their counterparts in rows 2 and 3). Also, the pressure levels on row 1 (posterior side) are much higher than those on row 4 (anterior side). This is a consequence of three-dimensional effects as a result of cross flows towards the posterior side that are caused by the sweep. The existence of these cross flows is also indicated by the initial dip in pressure along row 4, irrespective of the boundary layer thickness. Compared to the straight cavity case, the pressure levels towards the rear of the cavity show a marked increase.

ψ = 45°

The results of 45° sweep angle shown in Fig. 6(d) are dramatically different. Pressure values on the anterior side of the cavity (rows 3 and 4) initially drop before eventually increasing towards the trailing edge, due to the shear layer impingement. The initial drop, already seen in row 4 for the 15° sweep angle case, is much more pronounced now and even generates a zone with negative pressure on the anterior half of the cavity, which even extends into the posterior half (at x/l = 0·66, row 2 also registers a negative pressure). Furthermore, for both boundary layers the pressures on row 1 are much higher than those on row 4. The reason for this significant spanwise variation in pressure lies in the strong cross flows that exist at this large sweep angle. These pressure distributions suggest that the flow behaviour changes from the transitional open type to open along the span from anterior to posterior. The oil flow visualisation data (described later) are consistent with most of the features seen in the pressure records.

The secondary effect of the sweep is a spanwise increase in upstream fetch of the separating boundary layer, i.e., the spanwise increase of distance from the leading edge of the base plate and the associated increase of boundary layer thickness. This might also contribute towards the spanwise pressure variations.

3.5.2 Closed cavity results

ψ = 0°

Figure 7(b) shows pressure distributions on the floor for a straight closed cavity. The features to note are that, firstly, the boundary layer thickness effect appears to be insignificant. Secondly, the pressure distribution is typical of a closed cavity[8] (Fig. 7(a)), indicating initial flow separation, attachment on the floor, and finally reattachment at the trailing edge after separation in front of the rear face. Another notable feature of these measurements is that they show that the flow is remarkably two-dimensional.

ψ = 15°

The results for the 15° sweep angle (Fig. 7(c)) are very similar to those of the straight cavity showing that the small sweep has little effect. Both shape and values of the pressure distributions along the cavity differ only marginally from the ψ = 0° case. Again, the effect of boundary layer thickness on the pressure distributions is insignificant.

ψ = 45°

The results for the 45° sweep angle (Fig. 7(d)) are significantly different, both with respect to the shape of the distribution and the overall pressure values. For both thin and thick boundary layer cases, the results indicate a behaviour akin to a transitional closed cavity pressure distribution[8] (Fig. 7(a)), especially on the anterior side (rows 4 and 3), moving towards closed cavity behaviour on the

https://doi.org/10.1017/S0001924000002542 Published online by Cambridge University Press

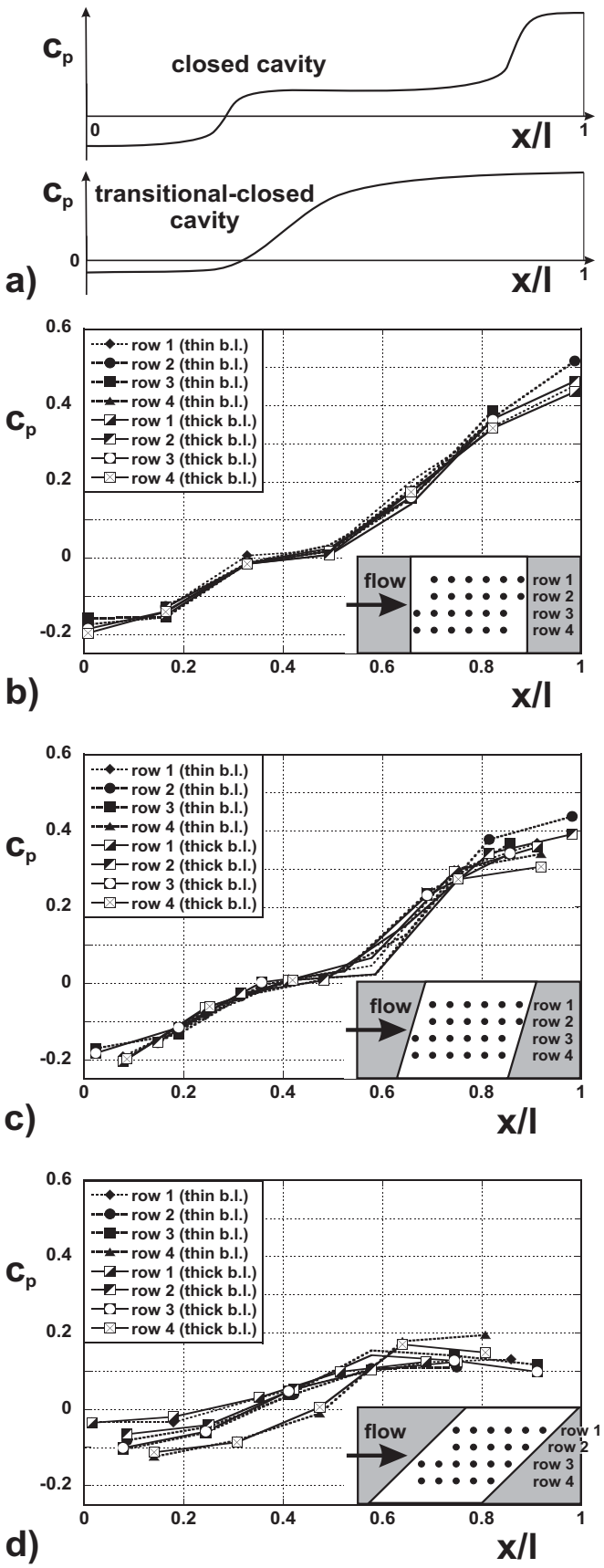


Figure 7. Steady pressure distribution in closed cavities (l/d = 16, M_∞ = 2) for thick and thin boundary layers (a) schematic of expected distributions for closed and transitional closed cavities[8], (b) straight cavity, (c) swept cavity, ψ = 15°, (d) swept cavity, ψ = 45°.

posterior side (rows 1 and 2), albeit with smaller pressure differences between front and rear part of the cavity. This again is a consequence of strong cross flows induced by the large sweep angle and is confirmed by the oil flow visualisation data. The progressively increasing pressures in the spanwise direction near the leading edge indicate the presence of cross flows impinging on the side walls and thus resulting in higher pressures. This effect is, however, less evident at the trailing edge where the impingement of the main flow on to the trailing edge becomes dominant. It is seen that the strong spanwise flow leads to an overall reduction of the pressures near the trailing edge. The pressures in the trailing edge region are seen to be nearly 50% of those measured for straight and 15° swept cavities.

3.6 Pressure distributions on cavity faces

As mentioned in Section 2, both the front and rear faces of the cavity were each equipped with 8 pressure ports in two rows of four in a staggered pattern, as indicated in the schematic sketch in Fig. 8. Both the top and bottom rows were positioned 1·5mm from the top and bottom edge of the cavity and the two farthest locations, spanwise, were each 20mm from the sidewalls of the tunnel. This helped to minimise the influence of the sidewall boundary layer. Because of the small depth of the cavity, only two pressure ports could be accommodated across the vertical direction of the face, so that the resolution with respect to cavity depth is somewhat coarse.

Figures 8(a), (b), and (c) illustrate pressure distributions on cavity front and rear faces which show some interesting features. These data were obtained with the natural boundary layer. Results obtained with a thicker boundary layer were virtually the same.

In the case of the straight cavity (ψ = 0°, Fig. 8(a)), the pressures on the front face for both open and closed cavities are almost uniform and show very good spanwise coherence. The rear face pressures, for the closed cavity, on the other hand, show considerable scatter, clearly the result of shear layer impingement and separation in front of the rear face. The other feature to note is the smaller pressure difference between the front and rear of the open cavity compared to that of the closed cavity. These measurements are consistent with the open and closed cavity mean pressure distributions obtained in previous studies[8].

With the 15° swept cavity (Fig. 8(b)), the results are similar to the straight cavity case, but the pressures on both the front and rear faces of the open cavity show an increase in the spanwise direction from the anterior towards the posterior side. A similar trend can be discerned on the rear face. As in the case of the straight open cavity, the difference in pressure on both faces is comparatively small.

The pressures on the front face of the closed cavity also show a slight increase from the anterior towards the posterior side, but overall they exhibit good spanwise coherence. The values are negative and similar to those measured for ψ = 0°. The rear face pressures show similar scatter as those in the straight closed cavity, and overall, the pressures are marginally lower.

Figure 8(c) shows the results for the 45° swept cavity. Here, the pressure variations are seen to be quite large across the span on both the front and the rear faces for both open and closed cavities. For the open cavity, the front face pressures on the anterior side show negative values, which is consistent with the trends seen on the cavity floor pressures. The rear face pressures also show large spanwise variations, which result from a combination of both the shear layer impingement and spanwise flow. The distribution of pressures on the front and rear faces of the open cavity are opposite to each other in the sense that pressures on the front face are higher midspan and lower near the sidewalls and those on the rear face are lower in the midspan region but higher towards the sidewalls.

The closed cavity pressures also indicate large variations on the front and rear face of the cavity. On the front face, a steep increase in pressure towards the posterior side is seen. The pressures are all negative and close towards the posterior, the pressure coefficient approaches zero. The pressures on the rear face show no such clear

https://doi.org/10.1017/S0001924000002542 Published online by Cambridge University Press

tendency and they are on average about 50% lower than in the ψ = 0° and ψ = 15° cases.

These results indicate that the overall effect of cross flows caused by the sweep is a pressure increase from the anterior side towards the posterior side. Depending on the initial pressure levels within the cavity and the type of cavity, the establishment of this pressure gradient can take two distinct forms: in an open cavity, the cross flows tend to lower the pressure on the anterior side of the front face and may even create zones of negative C_p values compared to the posterior side. The values of pressures on the rear face are less affected. The overall increase in pressure difference between the front and the rear face in an open swept cavity therefore stems mainly from the changes that occur on the front face across the span. By contrast, in a closed swept cavity, the cross flows lift the negative pressures on the front face towards positive values and at the same time reduce the positive pressures on the rear face. The net effect is a reduced pressure difference between the front and rear faces resulting in the reduced pressure drag of the cavity.

3.7 Cavity drag

An average value from the eight pressure ports was determined for both the front and rear face and this pressure was taken to be acting on each face. The time-averaged cavity pressure drag coefficient $\overline{C}_D$, neglecting skin friction on the floor, was then determined as[7];

$$\overline{C}_D = \frac{2}{\gamma M_\infty^{\,2}} \frac{d}{l} \int_0^1 \frac{\overline{p}_r - \overline{p}_f}{p_\infty} \mathrm{d}\left(\frac{z}{d}\right) \qquad \ldots (3)$$

where $\overline{p}_r$ and $\overline{p}_f$ are the average pressures on the rear and front faces of the cavity and p_∞ and M_∞ are the free-stream pressure and Mach number, respectively. z is the co-ordinate in vertical direction and d is the depth of the cavity, as indicated in Figs 1 and 8.

Figure 9 shows the variation of the drag coefficient $\overline{C}_D$ with sweep angle. For the open cavity, the $\overline{C}_D$ values so determined were 0·0075, 0·009, and 0·015 for the sweep angles ψ = 0°, 15°, and 45°, respectively, showing nearly a twofold increase in drag with sweep angle. The error in $\overline{C}_D$ due to inherent measurement inaccuracies is one order of magnitude lower than the error in C_p.

For the closed cavity, however, while there was no significant change in drag for the 0° and 15° swept cavities, a steep decrease in drag occurred with the 45° swept cavity. The $\overline{C}_D$ values were 0·039, 0·039, and 0·025, for ψ = 0°, 15°, and 45°, respectively. The sharp decrease in drag for the 45° swept cavity is due to the fact that the pressure drag is a consequence of the cavity being subjected to the normal flow Mach number $M_n = M_\infty \mathrm{Cos}\psi$ = 1·41 rather than M_∞ = 2. The data for the thicker boundary layer showed a similar trend and the values were almost identical. The results for ψ = 45° clearly show the importance of strong cross flows in calculating the cavity drag both from streamwise and spanwise components of pressures for finite span cavities with large sweep angles.

These results seem to indicate that overall, the introduction of sweep has the effect of reducing the difference in streamwise pressure drag between open and closed cavities. While for zero or small sweep angles (ψ < 15°) the drag of a closed cavity is higher by a factor of four to five compared to that of the open cavity, this difference is reduced to only about 60% for cavities with 45° sweep. This may have important implications in practice.

The evaluation of cavity drag from the pressure data on the front and rear cavity faces as described above is justified because the skin friction drag of the cavity floor is quite small compared to the pressure drag[7,16].

The present drag values for the straight (ψ = 0°) open and closed cavities are somewhat at variance with those presented by Charwat *et al*[7] at Mach 2. In particular, the open cavity value (l/d = 8) is about 50% of their estimate while that for the closed cavity is about 30% above. The only difference between the two cases is the ratio of

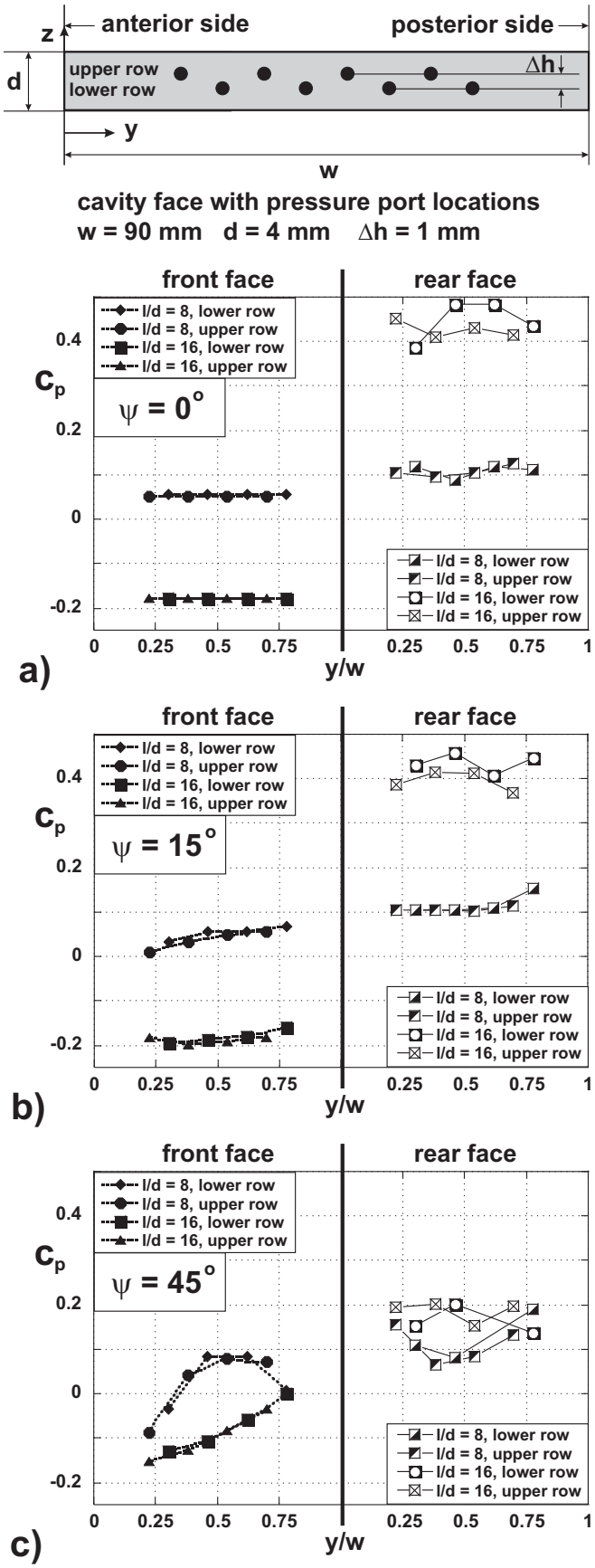


Figure 8. Pressure coefficients on the faces of the cavity (for thin boundary layer) (a) straight cavity, (b) swept cavity, ψ = 15° (c) swept cavity, ψ = 45°.

https://doi.org/10.1017/S0001924000002542 Published online by Cambridge University Press

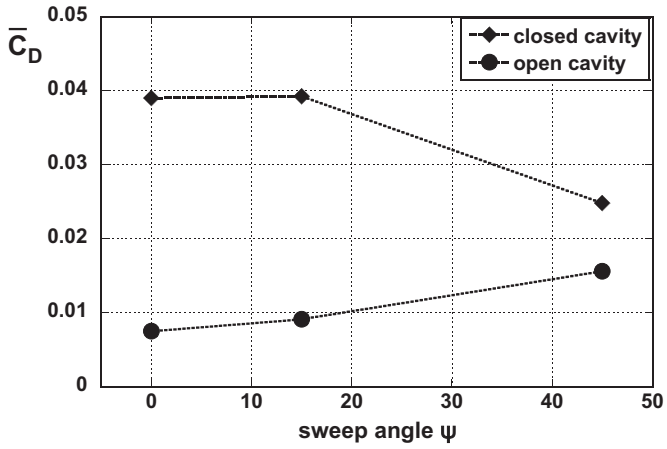


Figure 9. Time-averaged drag coefficient $\overline{C}_D$ as a function of sweep angle ψ.

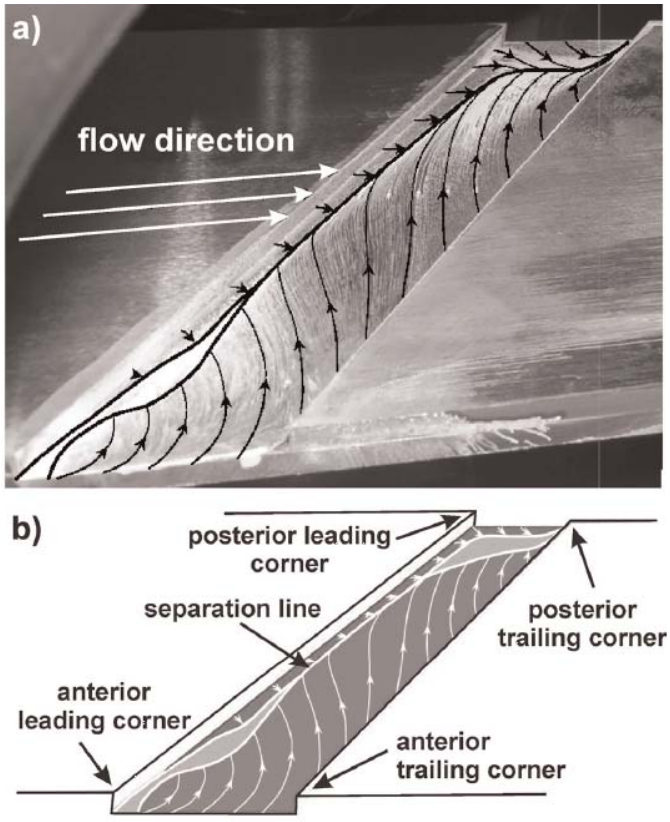


Figure 10. Surface oil flow patterns of the short swept cavity model: (a) actual flow pattern; (b) schematic.

boundary layer thickness to cavity depth, δ/d. In the present case, $0{\cdot}5 \leq \delta/d \leq 1{\cdot}0$, while Charwat *et al*[7] have $\delta/d >> 1$. Charwat *et al* further state that their drag estimates were made by 'smoothing out' the pressures measured on the rear face and then making the approximation that the front corner pressure was the same as that acting on the entire front face of the cavity. Secondly, McGregor and White[17] have shown that the drag coefficient is a strong function of δ/d and their calculations show that the drag coefficient increases with decreasing δ/d for a given Mach number. According to their calculations, the drag coefficient for the present straight open cavity should be 0·005, which is 33% lower than the measured value. However, it should be noted that the theory of McGregor and White[17] seems mainly to be applicable to short open cavities ($l/d \leq 3$) although they do not explicitly state this. Suffice to say that reliable measurements and predictions of shallow cavity drag covering both open and closed regimes even at 0° sweep are still sparse.

Finally, a comment needs to be made about the estimation of drag values of swept cavities. It is quite clear that because of the side walls and finite span of the cavities, there will be a cross flow component of the total drag which has not been accounted for as there was no provision for pressure tappings on the side walls (which are glass windows). For small sweep angles (≤ 15°) this component of the total drag can be expected to be quite small while for higher sweep angles it will be significant. Nevertheless, the results show that extension from two-dimensional to the swept case may be justified in case of small angles of yaw without recourse to the interdependence of the spanwise and chordwise flow. In their investigation of low speed flow over three-dimensional rectangular cavities at yaw, Savory *et al*[18] found that the effect of yaw on the overall drag coefficient was reduced as the cavity became more two-dimensional (i.e. increased in span). This they attributed to the reduced end wall effects. They also found that drag coefficients remained largely constant for yaw angles up to 30°.

3.8 Flow visualisation

3.8.1 Oil flow patterns

Oil flow visualisation experiments were conducted on the 45° swept cavity, both open and closed. This was done to visualise the effects of cross flows that were clearly evident from pressure data.

Figures 10(a) and (b) show the actual flow pattern and the corresponding schematic with details of the flow in the open swept cavity. From Fig. 10(a), it is apparent that the flow in the cavity is dominated by strong cross flows from the anterior towards the posterior. Although there is some interaction between the corner flows (both anterior and posterior) with the side wall boundary layers, the flow in the mid-span region quite clearly indicates a separated region incorporating a counter-clockwise vortex immediately downstream of the cavity leading edge. The streamlines past this region indicate the footprint of the main clockwise vortex spanning the cavity consistent with the open type cavity flow. It is interesting to note that this flow bears a striking resemblance to the flow over an infinitely swept wing at high angle-of-attack with leading-edge separation bubble and an attachment line[19]. The flow behaviour in the open swept cavity therefore is similar to the straight open cavity but is highly skewed because of the cross flows.

Figures 11(a) and (b) show the results pertaining to the closed swept cavity. The flow pattern is obviously quite different to that of an open swept cavity. The pattern on the anterior shows a flow akin to that of a transitional closed cavity in that there is a recirculating flow immediately after the leading edge separation, an attached flow combined with some developing cross flows and another recirculating region at the rear of the cavity. The figure also shows strong interaction between the side wall boundary layer and the anterior cavity flow. In the mid-span region, strong cross flow streak lines become less distinct and the flow appears more (uniformly) smeared. Then, on the posterior side, the flow is consistent with a closed type cavity behaviour. It would appear that the flow in the closed swept cavity undergoes changes across the span, from transitional-closed to a closed type flow.

3.8.2 Schlieren images

Figures 12(a) and (b) show direction-indicating colour schlieren images of open and closed cavities with 15° sweep angle. In these visualisations, unlike in the standard straight-knife-edge schlieren technique, all gradients normal to the optical axis become visible. Colour was used to code the direction of the encountered density

https://doi.org/10.1017/S0001924000002542 Published online by Cambridge University Press

gradients[20]. As noted earlier, schlieren visualisation was only possible for the straight and 15° swept cavity.

The boundary layer on the surface leading up to the cavity appears in the given colour coding as violet. The subsequent shear layer forming at the leading edge is characterised by approximately the same density gradient direction and thus the same colour. In the open cavity flow (Fig. 12(a)), the shear layer slightly deflects upwards forming a cavity leading edge shock. It subsequently thickens and bridges the cavity before impinging on the trailing edge. This gives rise to a small vortex at the upper corner of the trailing edge, seen as a combination of blue, green, and violet. Such a pattern is an indication of vorticity[20]. As a consequence of the shear layer impingement, pressure waves are set up propagating upstream towards the leading edge thus setting off the oscillatory mechanism. The waves oscillating within the cavity are essentially transient strong acoustic waves and will therefore only become fully visible in a time-resolved visualisation. Stationary flow features such as the trailing edge shock and expansion zones, on the other hand, are well defined and clearly visible in the present single-shot records.

The visualisation of the closed cavity flow (Fig. 12(b)) shows the shear layer separating from the leading edge, causing a strong expansion fan, and then attaching to the cavity floor. It separates again in front of the rear face before reattaching at the trailing edge. The attachment of the shear layer on the cavity floor causes an attachment shock which recompresses and redirects the flow parallel to the cavity floor. This shock is seen as a dark line embedded in a green zone, which signifies compression towards the cavity floor. In a straight cavity, this feature appears in almost identical fashion. The influence of the sweep only becomes obvious in the subsequent separation of the shear layer as it approaches the trailing edge. In a straight cavity, the separation leads to a narrow and distinct separation shock and the attached shear layer has a well-defined edge and an essentially constant thickness up to the location of the reattachment shock. By contrast, the spanwise variations in the swept cavity change this pattern into a broader, smeared-out compression region, as seen in Fig. 12(b). Upon the onset of the compression region, the edge of the shear layer becomes diffuse and its thickness appears to decrease initially. Close to the trailing edge, one can again notice a slightly distorted circular colour pattern indicating a vortical flow[20]. In corresponding images of a straight cavity, this vortex appears more pronounced and without distortions. As the schlieren technique provides a line-of-sight measurement, flow features that co-exist in spanwise direction are seen superimposed indicating that the vortical structure is changing its shape along the span. The schlieren images, when viewed in conjunction with the results of oil flow visualisation, broadly confirm the spanwise features of the flow inferred from the pressure data.

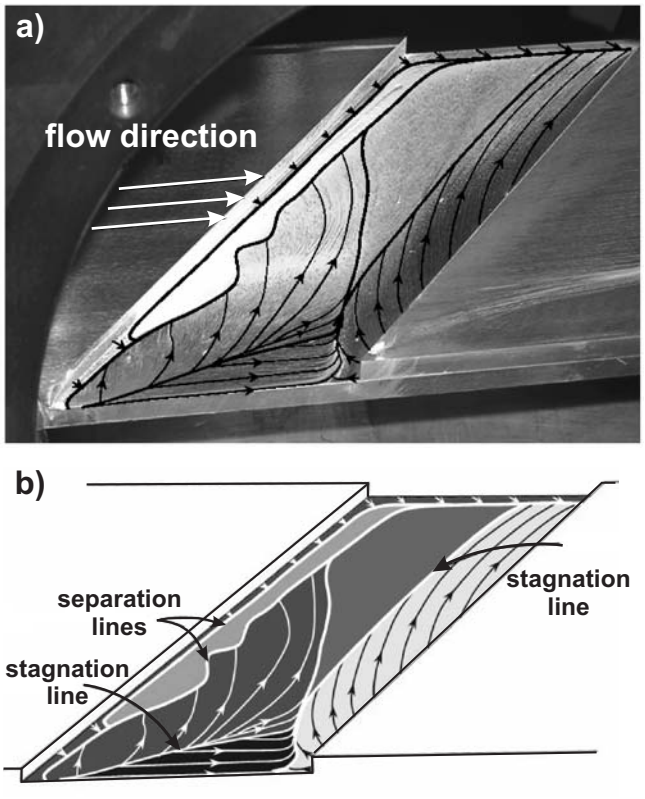


Figure 11. Surface oil flow patterns of the long swept cavity model: (a) actual flow pattern; (b) schematic.

4.0 SUMMARY AND CONCLUSIONS

4.1 Unsteady pressure field

In the case of an open swept cavity, the straight (0°) and the 15° yaw angle results both showed discrete resonant tones while the 45° yaw angle cavity showed a broadband spectrum with no discrete frequencies. The agreement between the calculated and experimental Strouhal numbers was very good for the second, third, and fourth Rossiter modes for the straight cavity but with the increase in yaw, the agreement became poor. Also, for a given mode, there was a trend towards a small increase in Strouhal number with increase in yaw. In the case of the closed swept cavity, no discrete frequencies were observed in the spectra at all yaw angles tested and also the average sound pressure levels were lower than those of the open cavity.

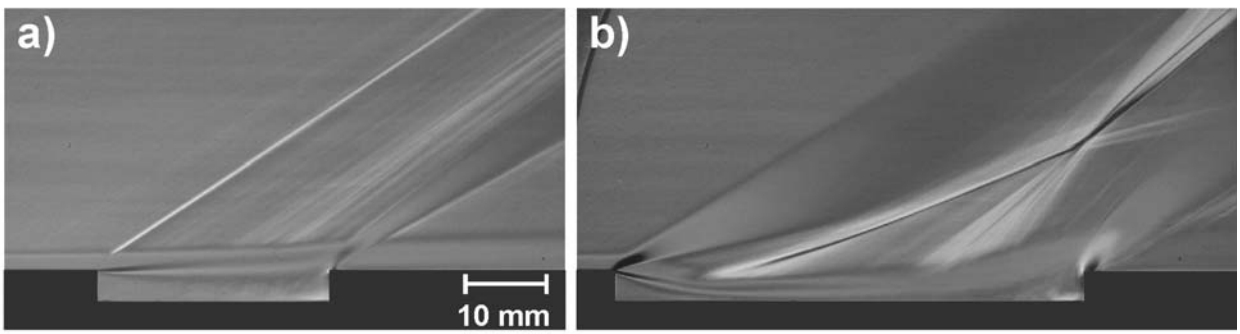


Figure 12. Direction-indicating colour schlieren images of the flow in open (a) and closed, (b) swept cavities at ψ = 15°.

https://doi.org/10.1017/S0001924000002542 Published online by Cambridge University Press

4.2 Steady pressure field

For the open swept cavity the 0° yaw results were consistent with the type of pressure distribution that had been obtained for straight open cavities in previous studies. The results from the 15° swept cavity showed small cross flow effects, but generally a similar distribution. With 45° sweep, however, these cross flow effects were accentuated and the flow behaviour changed from transitional open to open along the span.

With the closed swept cavity, the straight (0°) cavity results were consistent with previous studies. The 15° swept cavity results were similar to those of the straight cavity showing that the small sweep had little effect. The 45° case showed again significant differences from that of the straight cavity. As a consequence of strong cross flows induced by the large sweep angle, the flow changed from transitional closed to closed type along the span. This transition in behaviour was confirmed by the oil flow visualisation data.

4.3 Cavity drag

Based on time-averaged pressure measurements and within the constraints imposed by having only a limited number of pressure tappings on the faces of the cavity and none on the side walls, the results indicated an increase in drag with the sweep angle for the open type cavity. Between sweep angles of 0° and 45° the drag nearly doubled. With the closed cavity, however, while there was no significant change in drag between the 0° and 15° swept cavities, the drag decreased by nearly 37% for the 45° swept cavity. The difference in drag between closed and open cavities diminished with sweep angle, from a factor of 4 to 5 at small yaw angles (≤ 15°) to only 1·6 at the largest tested yaw angle of 45°. Changes of approximately 60% in the approaching boundary layer thickness had only negligible effect on the drag.

ACKNOWLEDGEMENTS

The authors would like to express their sincere gratitude to the members of the Mechanical Workshop of the School of Aerospace, Civil and Mechanical Engineering, in particular to Stuart Gay and Michael Jones, for their excellent technical support during this project.

REFERENCES

1. MALMOUTH, N.D. Theoretical aerodynamics in today's real world: opportunities and challenges, *AIAA J*, 2006, **44**, pp 1377-1392.
2. DOWLING, A.P. and HYNES, T. Towards a silent aircraft, *Aeronaut J*, 2006, **110**, (1110), pp 487-494.
3. KRISHNAMURTY, K. Acoustic radiation from two-dimensional rectangular cutouts in aerodynamic surfaces, 1955, NACA TN 3487.
4. TAM, C.K.W. and BLOCK, P.J.W. On the tones and pressure oscillations induced by flow over rectangular cavities, *J Fluid Mech*, 1978, **89**, pp 373-399.
5. GHARIB, M. and ROSHCO, A. The effect of flow oscillations on cavity drag, *J Fluid Mech*, 1987, **177**, pp 501-530.
6. ROSSITER, J.E. Wind-tunnel experiments on the flow over rectangular cavities at subsonic and transonic speeds, October 1964, ARC R&M 3438.
7. CHARWAT, A.F., ROOS, J.N., DEWEY, F.C. and HITZ, J.A. An investigation of separated flows – part 1: the pressure field, *J Aerospace Sc*, 1961, **28**, pp 457-470.
8. TRACEY, G.S. and PLENTOVICH, E.B. Characterization of cavity flow fields using pressure data obtained in the Langley 0·3 meter transonic cryogenic tunnels, 1993, NASA TM 4436.
9. STALLINGS, R.L. Store separation from cavities at supersonic flight speeds, *J Spacecraft and Rocket*s, 1983, **20**, pp 129-132.
10. ZHANG, X. and EDWARDS, J.A. An investigation of supersonic oscillatory cavity flows driven by thick shear layers, *Aeronaut J*, 1990, **92**, pp 355-364.
11. DISIMILE, P.J. and ORKWIS, P.D. Sound-pressure-level variations in a supersonic rectangular cavity at yaw, 1998, *J Propulsion and Power*, **14**, pp 392-398.
12. TOY, N., DISIMILE, P.J. and SAVORY, E. Local shear stress measurements within a rectangular yawed cavity using liquid crystals, *Optical Diagnostics in Eng*, 1999, **3**, (1), pp 91-101.
13. CROCCO, L. and LEES, L. A mixing theory for the interaction between dissipative flows and nearly isentropic streams, *J Aeronaut Sciences*, 1952, **19**, pp 181-208.
14. HOWE, M.S. *Acoustics of Fluid-Structure Interactions*, 1998, pp 453-456, Cambridge Univ Press.
15. ZHUANG, N., ALVI, F.S., ALKISLAR, M.B, and SHIH, C. Supersonic cavity flows and their control, *AIAA J*, 2006, **44**, pp 2118-2128.
16. SQUIRE, L.C., and NASSER, S.H. Cavity drag at transonic speeds, *Aeronaut J*, 1993, **95**, pp 247-256.
17. MCGREGOR, O.W. and WHITE, R.A. Drag of rectangular cavities in supersonic and transonic flow including the effects of cavity resonance, *AIAA J*, 1970, **8**, (11), pp 1959-1964.
18. SAVORY, E., TOY, N., DISIMILE, P.J. and DIMICCO, R.G. The drag of three-dimensional rectangular cavities, *Applied Scientific Research*, 1993, **50**, pp 325-346.
19. DAVIS, R.L., CARTER, J.E. and RESHOTKO, E. Analysis of transitional separation bubbles on infinite swept wings, *AIAA J*, 1987, **25**, pp 421-428.
20. KLEINE H. Flow visualization. In: BEN-DOR, G., IGRA, O. and ELPERIN, T. (Eds) *Handbook of Shock Waves*, **1**, pp 685-740, Academic Press, 2001.

https://doi.org/10.1017/S0001924000002542 Published online by Cambridge University Press